Matching and Control Optimization of Variable Geometry Turbochargers with Hydrogen FCEVs

Matt L Smith * , Alexander Fritot , Davide Di Blasio , Richard Burke , Tom Fletcher

Posted Date: 5 March 2025

doi: 10.20944/preprints202503.0334.v1

Keywords: Fuel cell electric vehicle; PEM fuel cell; turbomachinery; optimization; hydrogen vehicle; turbo matching; 1D modelling

Article

Matching and Control Optimization of Variable Geometry Turbochargers with Hydrogen FCEVs

Matt L Smith *, Alexander Fritot, Davide Di Blasio, Richard Burke and Tom Fletcher

University of Bath, Claverton Down, Bath, BA2 7AY, United Kingdom; acf49@bath.ac.uk (AF); ddb35@bath.ac.uk (DDB); en3rdb@bath.ac.uk (RB); tpf25@bath.ac.uk (TF).

* Correspondence: ms3510@bath.ac.uk

Abstract: Turbocharging of hydrogen fuel cell electric vehicles (FCEVs) has recently become a prominent research area, aiming to improve FCEV efficiency and viability to help decarbonise the transport sector. This work compares the performance of electrically assisted variable-geometry-turbocharging (VGT) with a fixed-geometry turbocharger (FGT) by optimising both the sizing of the components and their operating points, ensuring both designs are compared at their respective peak performance. A MATLAB-Simulink reduced-order model is used first to identify the most efficient components which match to the fuel cell air-path requirements. Maps representing the compressor and turbines are then evaluated in a 1D flow model to optimise cathode pressure and stoichiometry operating targets for net system efficiency, using an accelerated genetic algorithm (A-GA). Good agreement was observed between the two models' trends, with negligible difference in system efficiency and modelled shaft speed under optimised conditions. However, a sensitivity study demonstrates significantly higher efficiency when operating at non-ideal flows and pressures for the VGT when compared to the FGT, suggesting that VGTs may provide higher level of tolerance under variable environmental conditions such as ambient temperature, humidity, and transient loading. Overall, it is concluded that the efficiency benefits of VGT are marginal, and therefore not necessarily significant enough to justify the additional cost and complexity that they introduce.

Keywords: fuel cell electric vehicle; PEM fuel cell; turbomachinery; optimization; hydrogen vehicle; turbo matching; 1D modelling

1. Introduction

Hydrogen powered fuel cell electric vehicles (FCEVs) provide an opportunity to ease transport pollution due to zero tailpipe emissions [1] and the possibility to be powered by 'green' hydrogen, which is generated using renewable energy and feedstock [2]. As the automotive industry seeks to move away from fossil fuel powered vehicles and towards electrified powertrains, FCEVs provide a promising alternative for the heavy-duty vehicle market [3]. In particular, proton exchange membrane fuel cells (PEMFCs) are favoured for automotive applications due to high efficiency, high current density and low operating temperature, providing quick start-up [4,5].

To achieve maximum power density from the fuel cell stack, PEMFCs are commonly operated under pressurised conditions (up to ~4 bar [6]), allowing for better performance [7,8] and a reduction in stack size [9] . Fuel cell performance and efficiency increases as the pressure of the gases in the reaction increases as described by the Nernst equation [10] and can be observed experimentally [11–13]. Although there is an increase in stack power output, pressurising the system leads to significant parasitic loss to power the compressor. This can account for up to 80% of all parasitic losses experienced [14] and can require 15-35% of all power output from the stack [4,6,8,15,16].

To compensate for some of the losses from powering the compressor, a turbine can be used to recover some of the exhaust energy at the cathode outlet to drive the compressor shaft, reducing the power requirements from the e-motor. In contrast to an internal combustion engine, there is not

 doi:10.20944/preprints202503.0334.v1

enough energy in the exhaust flow to fully power the compressor [17]. However, up to 60% of the compressor power can be offset depending on operating conditions, resulting in increases in full system efficiency by up to 8% [7,18,19–21]. Existing findings are summarised in Table 1.

Table 1. Studies on the system efficiency benefits of FCEV turbine use compared.

Reference	Low/part load sys. eff. improvement	High load sys. eff. improvement	Compressor power offset by turbine
Martinez-Boggio et al. 2023 [18]	+1%	+8%	Up to 60%
Ahsan et al. 2021 [19]	+6% (approx.) across the operating range.		43.1-47.9% (approx.)
Filsinger et al. 2021 [21]			9%-39.3%
Kerviel et al. 2018 [7]	+3.3% (WLTP avg.) vs. single stage compressor +1.6% (WLTP avg.) vs. two-stage compressor		45.8% on average
Zhang et al. 2017 [20]		+6.9% (approx.)	25-44.7% (approx.)
Bao et al. 2006 [22]	+3% (approx.) vs. single stage compressor +1% (approx.) vs. two-stage compressor		
Kulp et al. 2002 [23]	+1% (approx.)	+5% (approx.)	
Cunningham et al. 2000 [24]	"Largely unchanged"	+4% (approx.)	

In internal combustion engine (ICE) vehicle applications, fixed geometry turbochargers (FGT) can experience lag in transient conditions such as low speed operation, due to the size of the turbine and its inertia [25]. Variable geometry turbochargers (VGT) overcome this by manipulating the effective aspect ratio of the turbine to reduce lag and increase the turbocharger's operating range, particularly increasing boost at low speeds and reducing over boosting [26]. VGT use with diesel engines can improve matching, enhance fuel economy, and reduce soot emissions [27] by increasing charge air mass by up to 20% compared to a FGT with wastegate [28].

For FCEVs, the reduction of lag and management of EGR for emissions reductions are no longer concerns. However, VGTs still offer potential benefits. Recent studies aim to leverage the extended operating range of VGTs for enhancing vehicle efficiency across a wider range of loads [9,17,21,29].

Several studies have found that VGTs can cover the full fuel cell operating range. Filsinger et al. [21] compared FGT and VGT at nominal air mass flow rates across a range of pressure ratios, as well as compromised (low and high) air mass flow rate conditions. At the nominal operating points (OP), they showed that FGTs recover more power due to their superior efficiency, but at the compromised, low and high mass flow rates, the VGT exhibited greater efficiency. The VGT appears to provide reasonable efficiency across the range, while the FGT peaks in the middle and drops at the extremes. Despite their improved performance at the extremes, the authors do not recommend VGT for most applications. Even at low mass flow rates where the absolute value of VGT power is greater than the FGT, the compressor consumes little power (6.3kW vs. 25.4kW for the highest load OP), so the proportion of power provided by the turbine is small and a FGT would be suitable. The main condition favouring VGTs is at high flow rates, where the VGT recovers more energy by utilising the full range of mass flow. But overall, the performance of two are similar across the operating ranges and the FGT with wastegate is recommended as a suitable and less complex solution.

Zhang et al. [9] also found that their bespoke VGT covers the full operating range whilst FGTs do not. Maximum energy recovery at low load was achieved using a FGT with wastegate (WG) and

 doi:10.20944/preprints202503.0334.v1

at high load with a FGT with back pressure valve (BPV), but their VGT performs well enough across all loads to maximise average efficiency.

Other studies conclude that VGTs should be redesigned for fuel cells to ensure that the full operating range is covered. For example, Menze et al. [17] and their subsequent paper Schoedel et al. [29] found that a VGT without wastegate can cover the entire operating range only if solidity (the ratio of blade chord to pitch) was reduced. They also find large performance improvements when doing so, reducing the inherent losses of VGTs pivoting vanes and reduced gaps to the housings [29]. This is similar to the findings of Taylor et al. [30], who found a 13% increase in VGT efficiency by modifying turbine wheel geometry vs. using an unchanged VGT from an ICEV.

The combined findings above indicate the importance of correctly sizing turbomachinery for fuel cells, whilst the control optimisation work by Bao et al. [22] and the influence of stoichiometry on system efficiency observed by Piqueras et al. [31], illustrate the importance of optimising the operating points. Zhao et al. [32] explain that the operating parameters of the fuel cell must be established before considering parameters of the turbine and compressor, for optimal matching. Mass flow rate and pressure demanded by the stack are fundamental parameters for matching [33], especially for mechanically coupled turbochargers, where the pressure ratio and mass flow rate ranges of the compressor and turbine must approximately correspond [34]. As the sizing of the turbomachinery will affect the optimal operating points for overall system efficiency, and the operating points will in-turn determine the correct sizing of components, these factors are inherently coupled, however no previous work has been identified which combines both optimisation of sizing and control concurrently.

The aim of this work is therefore to determine the performance of a PEMFC system when used with a VGT against a FGT. This differs from previous work in the area by concurrently considering both the selection of turbines and their operating points to ensure a comparison of FGT and VGT architectures when they are operating at their respective ideal performance.

The paper is structured as follows. Section 2 describes the approach taken to optimise both system design and operating point using a combination of reduced-order modelling in the FCMT and 1D model. Section 3 presents a comparison of the optimised results and related discussion to the overall performance comparison, control actuation and sensitivity. Finally, Section 4 summarises the conclusions and provides suggestions for further work in the area.

2. Materials and Methods

The methodology used in this study is an iterative cycle utilising two different models, as illustrated in Figure 1.

 doi:10.20944/preprints202503.0334.v1

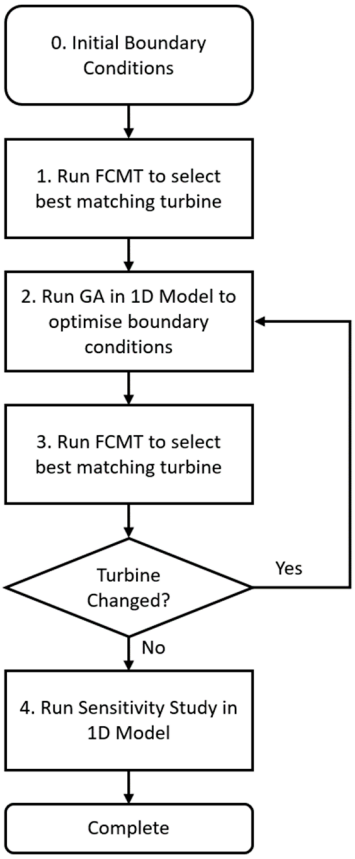

Figure 1. Methodology overview.

The first step utilises a reduced-order model to compare the performance of different turbine geometries based on prescribed boundary conditions within the Fuel Cell Matching Tool (FCMT). This uses a map-based approach to quickly assess each design, providing data on their power, speed, and turbine efficiency to identify the best match for the operating conditions provided.

The second step uses 1D modelling to dynamically simulate the fuel cell stack and air management system. This more detailed approach models the fuel cell system's thermo-/fluid dynamic properties to define the stoichiometry and inlet pressure of the fuel cell across a range of current densities in order to optimise system efficiency for the given turbine selected by the FCMT.

This methodology is iterated until the selection of the turbine remains unchanged and finally the 1D model is used to perform a sensitivity study. The following two sections describe the two numerical models in more detail.

2.1. Fuel Cell Air Path Matching Tool (FCMT)

The FCMT is used to select the best matching compressor and turbine for a given fuel cell stack and target operating conditions (stack inlet pressure and oxygen excess ratio) across a range of current densities. For this study, the compressor and fuel cell stack were pre-defined, the VGT was selected by the FCMT and the FGT turbine map was represented by the VGT operating with a "flush gap". This allows for fair comparison of the FGT and VGT architectures by ensuring they have the same efficiency characteristics and swallowing capacity.

The initial operating conditions were provided based on previous work [18] and consisted of a set of desired cathode inlet pressures and oxygen excess ratios (OER) for a range of 18 current densities from 0.05 A/cm^2 to 1.7 A/cm^2. These are used in conjunction with a set of parameters which describe the environment and the design of the airpath system (e.g., pressure drop across the fuel cell) to determine the boundary conditions for both compressor and turbine as follows.

 doi:10.20944/preprints202503.0334.v1

The boundary conditions for the compressor and turbine are defined by their pressure/expansion ratios and corrected air mass flow rates, which can be extracted directly from the 1D model results or calculated within the FCMT from the desired fuel cell operating conditions. The FCMT models pressure drop of the air inlet, intercooler, fuel cell stack and exhaust (illustrated in Figure 2) as fixed orifices based on Equation 1. The orifice area and discharge coefficient are summarised by parameter (k) which is automatically generated based on experimental data, as shown in Figure 3.

$$\Delta p = k \frac{\dot{m}^2}{\rho} \tag{1}$$

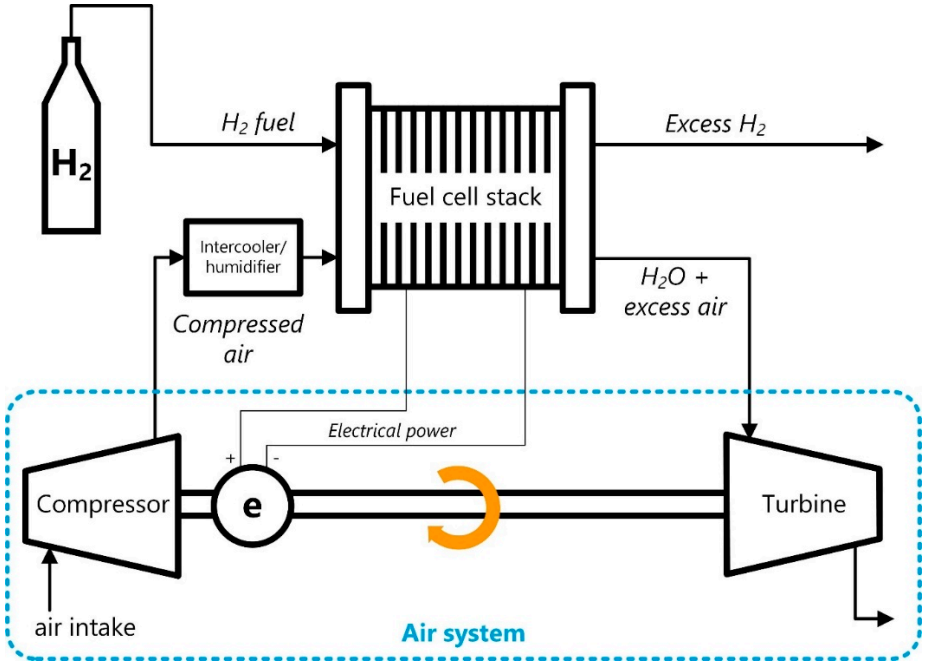

Figure 2. Fuel cell system diagram including definition of air system.

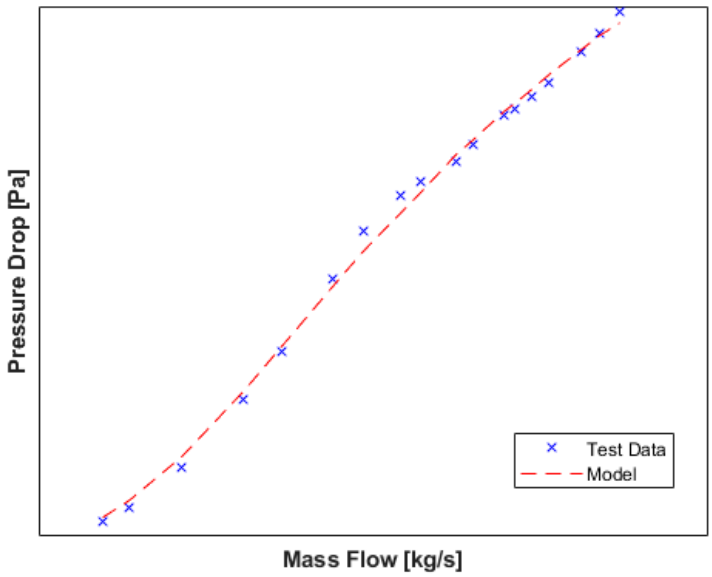

Figure 3. Orifice model of pressure drop.

 doi:10.20944/preprints202503.0334.v1

The mass flow through the compressor ($\dot{m}_{cmp}$) is calculated as the product of the OER (R_{EO}) and the required airflow ($\dot{m}_{\lambda}$) at the given current density (i), as described by Equation 2 and Equation 3.

$$\dot{m}_{cmp} = R_{EO}\dot{m}_{\lambda,air} \tag{2}$$

$$\dot{m}_{\lambda,air} = \left(\frac{100}{21}\right)\frac{in_cA_cM_{O2}}{4F} \tag{3}$$

It is assumed that the back-diffusion of water generated at the cathode through the membrane is negligible under steady state conditions, and therefore the mass flow through the turbine is calculated as in Equation 4 and Equation 5.

$$\dot{m}_{trb} = \dot{m}_{cmp} - \dot{m}_{\lambda,O2} + \dot{m}_{\lambda,H2O} = \dot{m}_{cmp} + \dot{m}_{\lambda,H2} \tag{4}$$

$$\dot{m}_{\lambda,H2} = \frac{in_cA_cM_{H2}}{2F} \tag{5}$$

Once the boundary conditions have been determined, the speed and efficiency of the compressor and turbine can be calculated using a map-based approach as described by SAE J922 [35] and J1826 [36]. This in-turn enables the calculation of mechanical work as in Equations 6-8 for the compressor and Equations 9-11 for the turbine.

$$T_{cmp,out,isn} = T_{cmp,in}\Delta p_{cmp}^{\frac{\gamma-1}{\gamma}} \tag{6}$$

$$P_{cmp,isn} = \dot{m}_{cmp} * c_p * (T_{cmp,out,isn} - 1) \tag{7}$$

$$P_{cmp,mch} = \frac{P_{cmp,isn}}{\eta(\dot{m}_{cmp,i}, \Delta p_{cmp})} \tag{8}$$

$$T_{trb,out,isn} = T_{trb,in}\left(\frac{1}{\Delta p_{trb}}\right)^{\frac{\gamma-1}{\gamma}} \tag{9}$$

$$P_{trb,isn} = \dot{m}_{trb} * c_p * (T_{trb,out,isn} - 1) \tag{10}$$

$$P_{trb,mch} = \frac{P_{trb,isn}}{\eta(\dot{m}_{trb,i}, \Delta p_{trb})} \tag{11}$$

Finally, the electric motor power is calculated based on the net mechanical power of the compressor and turbine, a fixed bearing efficiency and a map-based motor efficiency, as in Equations 12-14.

$$P_{EM,mech} = \frac{P_{cmp} + P_{trb}}{\eta_{bearing}} \tag{12}$$

$$P_{EM,elec} = \frac{P_{EM,mech}}{\eta_{EM}(N_{EM},T_{EM})} \quad \text{when motoring (and power is +ve)} \tag{13}$$

$$P_{EM,elec} = P_{EM,mech}\eta_{EM}(N_{EM}, T_{EM}) \quad \text{when generating (and power is -ve)} \tag{14}$$

The VGT is represented by a discrete number of nozzle gaps with a corresponding map for each. To match the speeds of the compressor and turbine, it is assumed by the tool that the VGT boundary conditions can be adjusted using either the nozzle gap, a back pressure valve or a wastegate as required. In the first instance, the nozzle gap will be optimised to control the fuel cell back pressure. If this is not possible, either the flow rate through the turbine is reduced by partially opening the

 doi:10.20944/preprints202503.0334.v1

wastegate, or a back pressure valve located after the turbine is partially closed to reduce the pressure ratio. This control scheme is shown in the right of Figure 4.

In the case of a FGT, only a back pressure valve or a wastegate are available. The wastegate and back pressure valve are represented by scaling the mass flow rate and expansion ratio (respectively) between 0% and 100% of the target conditions. To reduce the design space and simulation time, it is assumed that the wastegate does not open whilst the back pressure valve is partially closed, and vice versa (Figure 4, left).

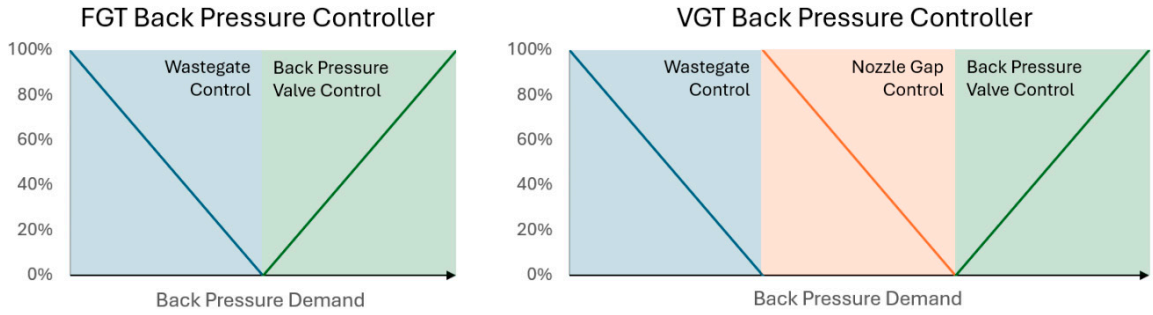

Figure 4. Control scheme for FGT (left) and VGT (right).

The FCMT runs the algorithm to estimate the performance of each turbine in a catalogue consisting of over 200 FGTs and approximately 30 VGTs. The final selected turbine is chosen based on the one which will minimise the electrical power requirement of the motor ($P_{EM,elec,i}$) across the weighted range of operating points, where (k_i) represents the weight of an individual operating point. The cost of each is found by Equation 15.

$$J = \frac{\sum_{i=1}^{n} k_i P_{EM,elec,i}}{n} \quad (15)$$

By using power rather than efficiency in Equation 15, the tool will inherently prioritise higher power operating conditions where the efficiency benefits are more significant. The operating point weighting enables users of the matching tool to prioritise particular operating points. However, for this work, it should be noted that the weighting of each point is kept equal in the interest of examining the performance of the VGT across the full range of operation.

2.2.1. D System Model

The 1D simulation model used for this work was developed based on the simulation model described in previous work by the authors [18], in which the air path design has been adapted to use a VGT. The base model was developed in GT-Suite (v2022, Gamma Technologies) and PEMFC calibration performed using manufacturer data. As shown in Figure 5, this model follows a similar structure to the reduced model in the FCMT, but each component is modelled at a higher fidelity using 1D-CFD, enabling the electro-chemical response of the fuel cell to varying pressure and flow rates to be evaluated. As with the FCMT, the mass flow rate is controlled using the electric motor and the backpressure is controlled using the state-based control scheme shown in Figure 4. For more information about this model, including its validation, please refer to the earlier publication [18].

Preprints.org (www.preprints.org) | NOT PEER-REVIEWED | Posted: 5 March 2025 doi:10.20944/preprints202503.0334.v1

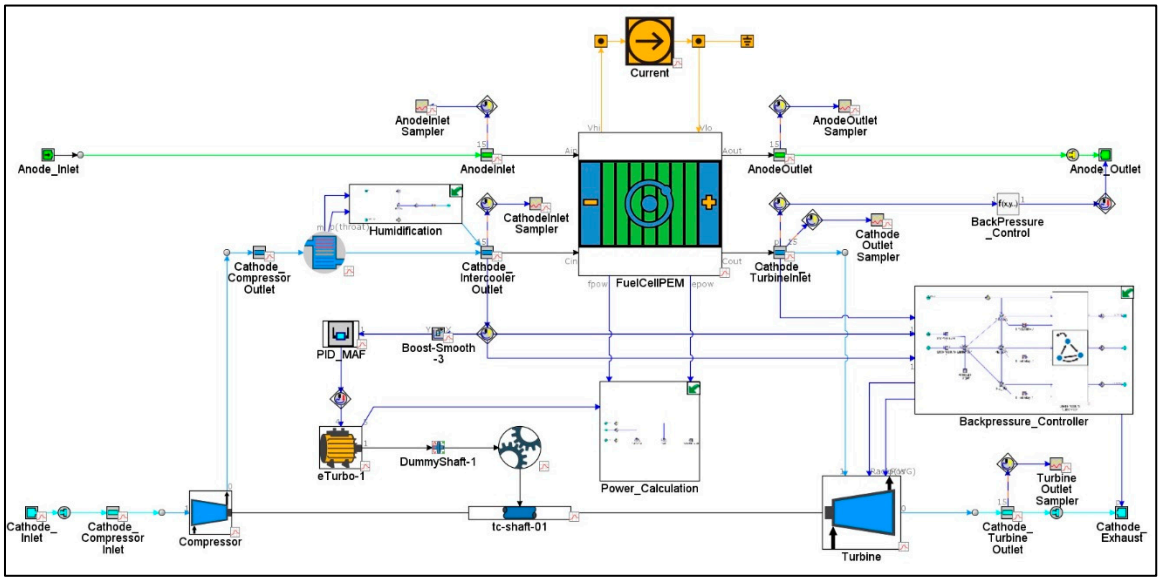

Figure 5. 1D GT-Suite model diagram.

2.2.1. Operating Point Optimisation

To ensure optimal operating conditions for both sets of turbines, numerical optimisation within GT Suite was conducted for the OER and turbine inlet pressures for both turbine geometries independently, with the aim to maximum net system efficiency at each current density operating point. Net system efficiency is defined in Equation 16.

$$J_i = \eta_{net,elec,i} = \frac{P_{FC,i} - P_{EM,i}}{\dot{m}_{H_2,i} \cdot LHV} \quad (16)$$

Optimisation was performed using the accelerated genetic algorithm, which is modified NSGA-III global search algorithm that incorporates fast metamodeling between each generation. Initial optimisation was performed for each current density across the full range of the compressor map using a population size of 10, for 15 generations. The crossover rate was 1, mutation rate of 0.5, crossover rate distribution index of 15, and a mutation rate distribution index of 20. This was then refined within +/-20% of the initial operating point locations, using a population size of 20 for 25 generations, with a crossover rate of 1, mutation rate of 1, crossover rate distribution index of 15, and a mutation rate distribution index of 10. The results of the second stage optimisation were also used to generate the contour plots shown in the sensitivity study results.

3. Results

3.1. 1D Modelling

The results from the 1D modelling indicate that fuel cell stack power is very similar whether a fixed geometry turbocharger (FGT) or variable geometry turbocharger (VGT) is used. This is shown in Figure 6, the lower left portion of which shows less than 1% difference in stack power across the range of current density operating points with use of FGT or VGT. The data also shows that the choice of FGT or VGT subsequently has negligible effect on overall system efficiency: Figure 6. shows less than 0.25% difference when using either turbocharger in the lower right.

 doi:10.20944/preprints202503.0334.v1

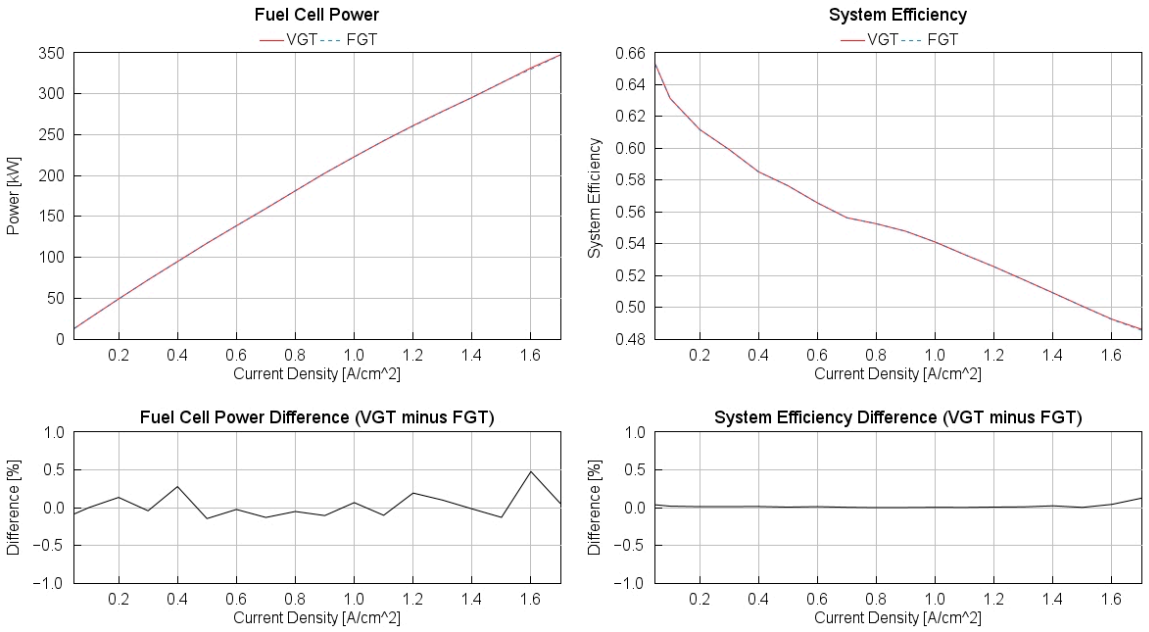

Figure 6. Comparison of fuel cell system performance parameters when using VGT and FGT.

The very similar system performance data – fuel cell power and overall system efficiency – when using either turbocharger is due to two main factors: fundamental turbo design, such as size, and turbine operating point, such as speed. The fundamental turbine design was purposefully kept the same in this study to ensure the effect of a variable nozzle gap was isolated. However, the turbine operating points were found by the boundary condition optimisation exercise, aiming to maximise overall system efficiency. This was conducted independently for FGT and VGT to assess if their optimal operation differs because of their different air system controls. It was found that the optimised operating points for the two turbos are similar despite their different control capabilities, as shown in Figure 7, where the FGT and VGT operate along the same curve for much of the operating range. A slight divergence is noticeable at the final two points, representing 1.6A/cm^2 and 1.7A/cm^2, where the VGT begins to curve downward, more closely following the peak efficiency curve of the compressor. It is also noticeable from these plots that the operating curve closely follows the peak efficiency curves of both compressor and turbine, demonstrating that the compressor and turbine are well matched to each other as well as to the fuel cell requirements.

Subsequently, this results in little difference in e-motor power, as shown in Figure 8, which also presents turbine inlet pressure and turbocharger shaft speed. The e-motor provides the remaining compressor power that is not provided by the turbine. Since the optimisation of the two turbines did not result in significantly different operating points, and because they have the same fundamental geometry and efficiency characteristics, they recover similar power across the range. Therefore, the remaining compressor power provided by the e-motor power is also very similar. As observed previously in Figure 6, this causes the overall system efficiency to be almost the same whether a FGT or VGT is used.

 doi:10.20944/preprints202503.0334.v1

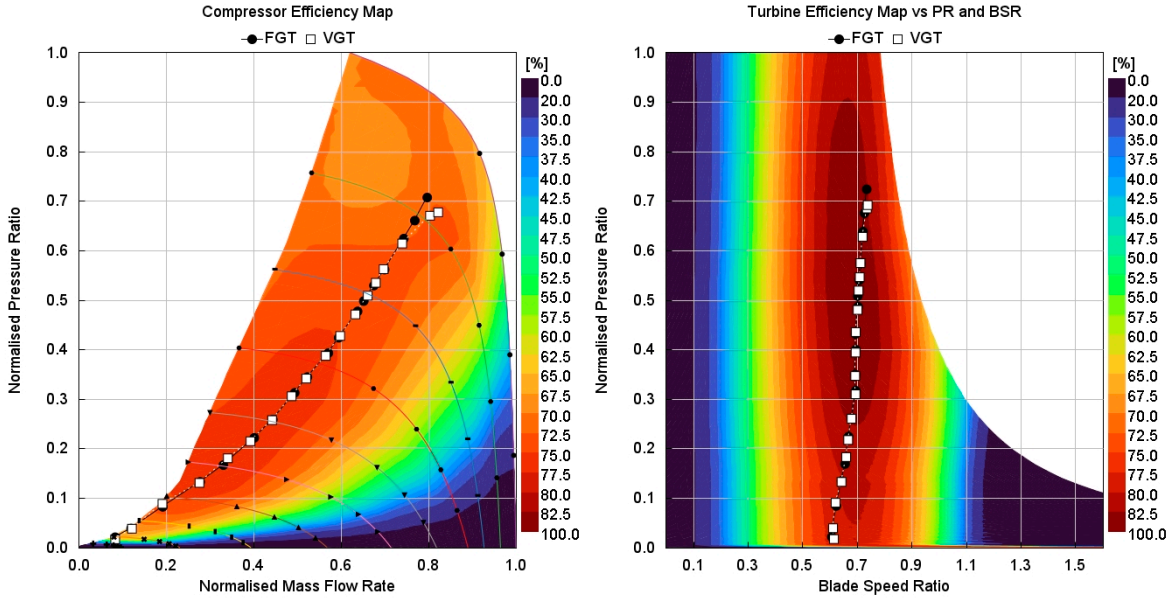

Figure 7. Optimised operating points overlaid onto compressor and turbine efficiency maps.

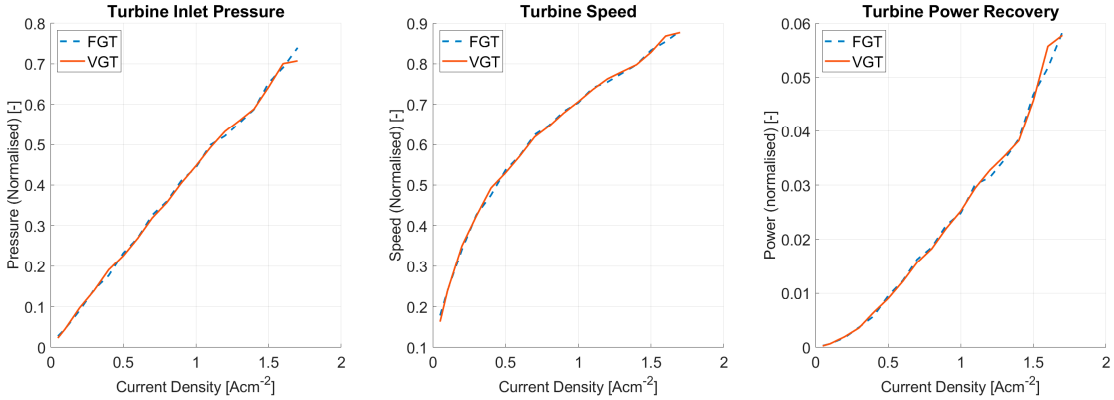

Figure 8. Optimised turbine inlet pressure and resulting shaft speed and e-motor power when using FGT and VGT.

Similar FGT and VGT operating conditions also results in very similar utilisation of the air system controls. For both turbos, Figure 9. shows that the magnitude of the controls used is very small, indicating negligible wastegate use by the FGT, minimal change in rack position by the VGT, and no use of the back pressure valve for either. As explained in the methodology, the VGT model was able to use the wastegate and back pressure valve if its rack position limits were reached. However, according to this data, the optimised rack position remains very near to the centre of the rack, comfortably between 45% and 60%, and exactly 51% for much of the current density range. Similarly, the FGT, represented by a constant rack position at flush gap (51%), required little wastegate to meet its optimised operating points.

 doi:10.20944/preprints202503.0334.v1

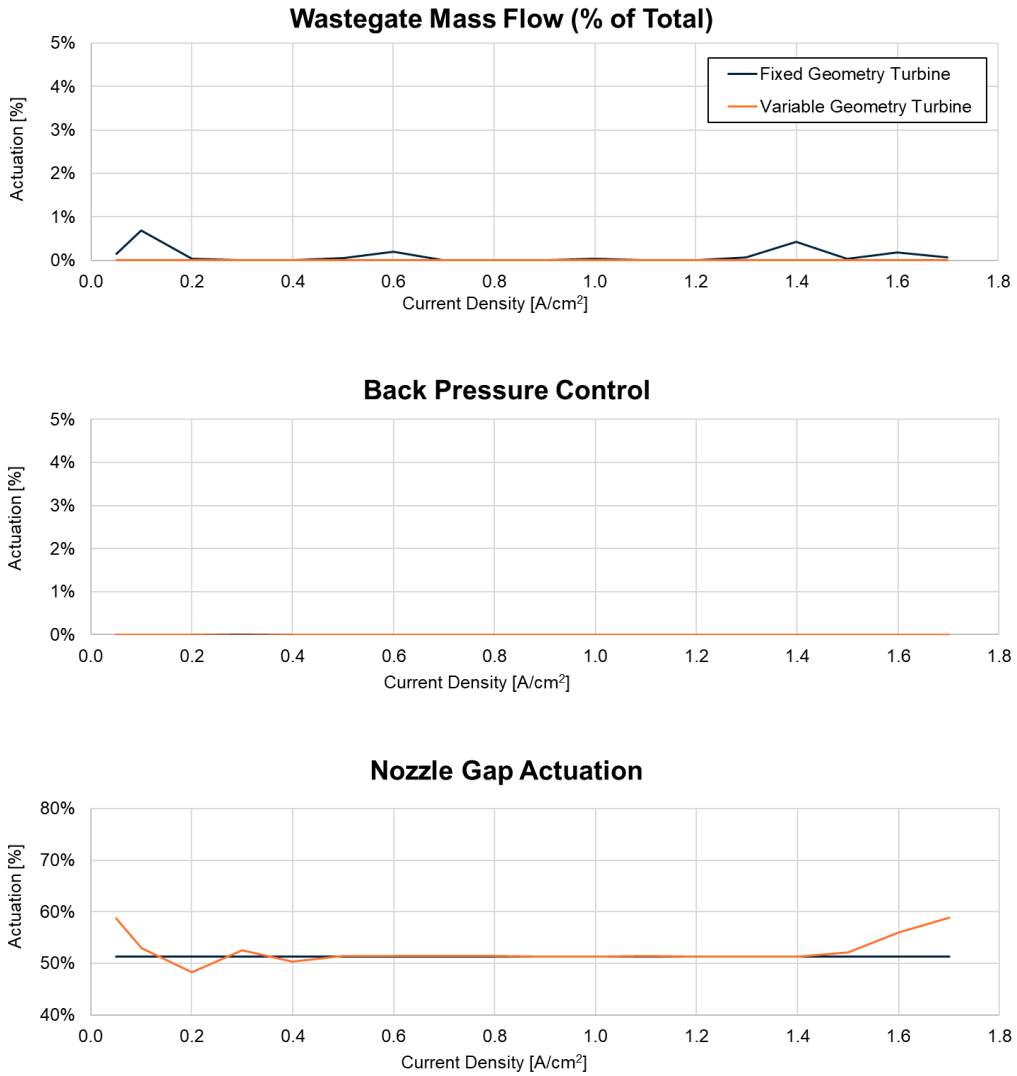

Figure 9. Use of air system controls compared for FGT and VGT.

3.2. Optimisation of Turbine Operating Points

The data presented above were generated using optimised turbine boundary conditions, found by the accelerated GA optimisation method described previously. This provides a series of target turbine inlet pressures and air mass flow rates, which are unique but very similar for the FGT and VGT, as explained. This section presents the results of the optimisation exercise itself, which indicate the sensitivity of each turbine to sub-optimal operating conditions.

Whilst the optimal boundary conditions are very similar for the two turbines, the VGT exhibits less reduction in fuel cell system efficiency when operating under sub-optimal boundary conditions. The contour plots in Figure 10. show the modelled inlet pressures vs. air mass flow rates during the optimisation exercise, with the colours representing the resulting fuel cell system efficiency. The upper three plots represent the system using the FGT, the lower three represent the VGT. From left to right are three current density operating points: 0.05 (idle), 0.9 (mid), and 1.7A/cm² (high). It can be seen that the high efficiency areas are larger in the VGT plot, showing less degradation in performance in sub-optimal operating conditions. This suggests greater resilience if operating in compromised conditions, such as due inadequate maintenance, or high altitudes. In contrast, for the FGT shows a more sudden drop in system efficiency under suboptimal conditions. These plots illustrate a vital, practical difference between FGT and VGT under real-world conditions which is not immediately apparent from the ideal, optimised results.

 doi:10.20944/preprints202503.0334.v1

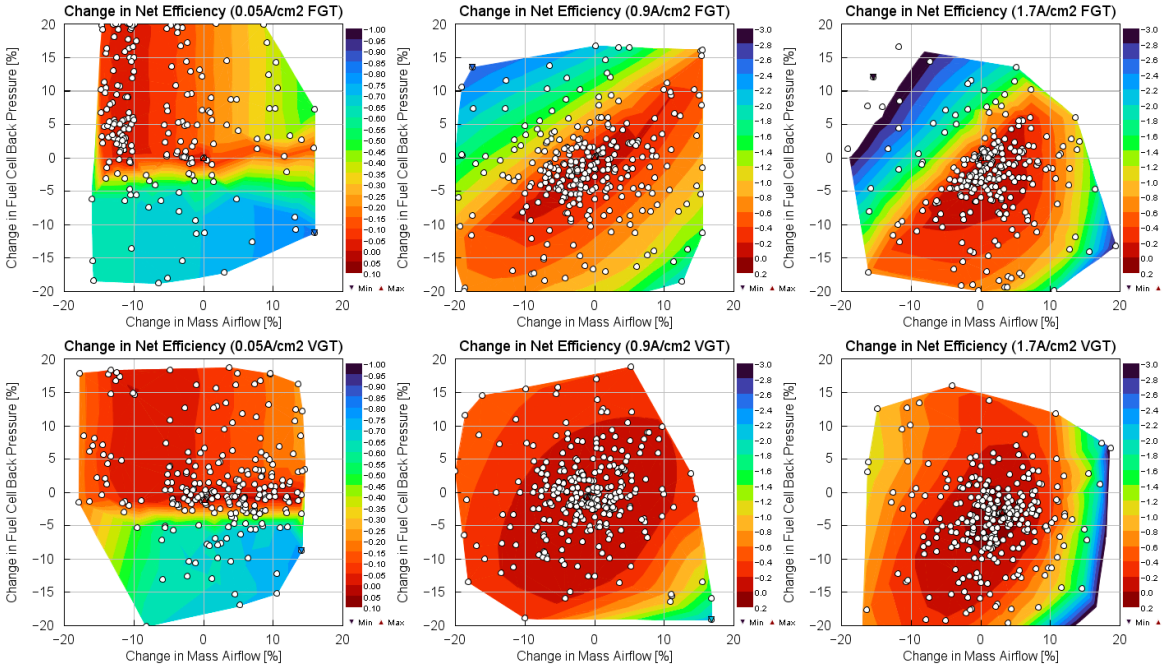

Figure 10. Sensitivity of FGT (top) and VGT (bottom) to variations in air flow and pressure target.

3.3. Matching Tool Results

This section compares the results from the fuel cell matching tool (FCMT) to those of the 1D modelling. Repeating the FCMT exercise with the optimised boundary conditions verified that the earlier turbine geometry selection remained the best choice. The performance data from the FCMT will be compared to that of the 1D model to support and understand the observations presented previously.

There is very good agreement in the results of the two models. In the FCMT results, the performance of the FGT and VGT appears to be very similar, validating the same observation in the 1D results. Figure 11 shows the FCMT results for shaft speed and net power (or e-motor power) of the two turbines from both modelling approaches: the FCMT results are shown in orange (solid line) for the VGT and blue (dashed line) for the FGT, while the results from the 1D model are shown in grey. It can be seen that the 1D and FCMT models predict almost identical shaft speeds, resulting in similar e-motor power. Both models predict similar trends in the data, however the reduced order modelling in the FCMT estimates approximately 4% lower motor power at full load.

 doi:10.20944/preprints202503.0334.v1

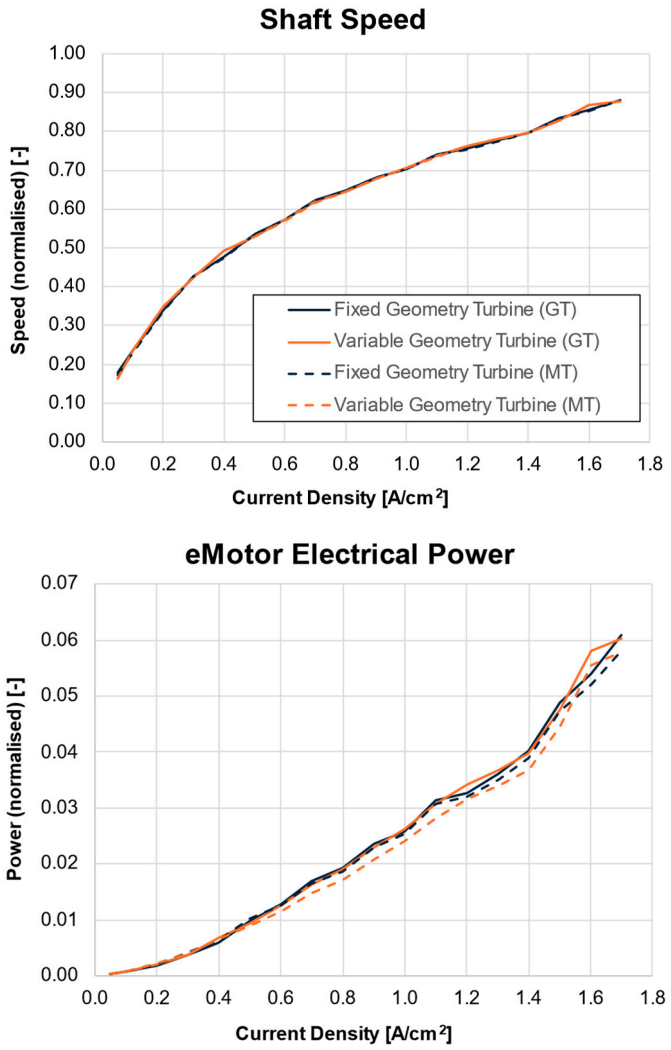

Figure 11. Performance results from matching tool study compared to 1D study.

This close alignment of the FCMT and 1D models' results is also observed in the use of controls. As described, the 1D model found that the FGT and VGT achieve their system-optimal operating points with negligible use of the rack position, and wastegate and back pressure valves. The same trend is observed in the FCMT results as shown in Figure 12. However, it can be seen that the matching tool estimates a slightly higher wastegate mass flow for the FGT, and similarly, estimates a slightly higher nozzle opening for the VGT.

 doi:10.20944/preprints202503.0334.v1

Figure 12. Control results from matching tool study compared to 1D study.

4. Discussion

The aim of this study was to assess whether a well matched VGT was able to outperform a FGT over the full range of current densities of a modern fuel cell stack. Our results show that VGTs deliver negligible benefit compared to FGTs when used with fuel cell powertrains under optimised operating conditions. The results suggest that the additional degree of control freedom offered by the VGT, the nozzle gap, does not inherently result in enhanced system efficiency at any point across the fuel cell stack operating range, and that both turbines were capable of operating at high efficiency across the full range of conditions.

The similarity in FGT and VGT performance observed is explained by control actuations used to meet the optimised operating conditions. For the VGT, these are achieved using a nozzle gap between 48-59% across the full range of testing. A VGT operating with only a small range of rack positions is operating somewhat similar to a FGT, so results in similar VGT and FGT performance. The minimal range of rack positions is also centred around 51%, which for the VGT in the study represents the 'flush gap'. The flush gap typically provides the best turbine performance and, in this study, also represents the FGT. Similarly, the FGT controller used minimal intervention from either a wastegate or back pressure in order to achieve its optimised operating conditions.

The minimal intervention of fuel cell pressure control, including the nozzle gap, wastegate, and back pressure valve indicate that the matching exercise was effective. Little variance in rack position around the flush gap suggests that the VGT remains comfortably in an efficient part of its operating window, whilst meeting the air system requirements. The FGT similarly requires little use of the

 doi:10.20944/preprints202503.0334.v1

wastegate and back pressure valve to meet its operating requirements, the use of which would result in system efficiency losses. This shows that the air flow characteristics such as mass flow rate and pressure do not need to be modified significantly, and hence the turbines are well matched and sized for this fuel cell system. It is debated in the literature whether either kind of turbine can meet the full range of fuel cell air system requirements, however, this study indicates they can when both component sizing is well matched to the application and operating conditions are optimised. This verifies the importance of matching (and air system design generally) in conjunction with optimal control. These two distinct areas of the literature were identified to construct the aim of this work.

Despite the various similarities in performance of the FGT and VGT, the key difference between the two architectures is their robustness to sub-optimal boundary conditions. The operating point optimisation exercise illustrated how the fuel cell system efficiency quickly reduces when the FGT is operated away from its optimal operating points, compared to when using the VGT, when the system efficiency is much more stable. A small deviation from the optimal inlet conditions would result in a smaller penalty in vehicle efficiency when using a VGT than a FGT. Therefore, the choice of VGT for a FCEV may not provide a performance benefit over FGT but appears to be more resilient to sub-optimal air conditions such as altitude. These results correlate to those of Filsinger et al. [21], however, in this work we have also shown that the VGT is resilient to deviations in pressure as well as in air flow rate.

In contrast to Zhang et al. [9], this study showed that both FGT & VGT were able to operate at high efficiency across the full range of current densities. One area where there was a small difference in the target operating point was at the two highest current densities, where the VGT showed a 0.25% improvement in system efficiency due to more closely following the peak efficiency of compressor efficiency map. This is likely due to the higher robustness of the VGT when operating at compromised operating points. This hints that the FGT may be operating closer to its limit at these points and could exhibit a loss in efficiency if tested at higher electrical loads.

Overall, this study shows the importance of combining optimised control with optimal air system matching and design. The results broadly agree with the literature, which demonstrates the importance of design and control separately, whilst this study combines them. Optimising in design and control simultaneously, under the assumption of steady state conditions suggests that VGTs are not worth the additional cost and complexity, demonstrating just 0.25% improvement in efficiency at peak load, and negligible improvement at other current densities.

5. Future Work

Certain limitations of this work should be noted. Firstly, the matching exercise in this study was conducted for the VGT only and the FGT was represented using the ‘flush gap’ map of the VGT. This was performed to isolate the effect of variable geometry and eliminate other potential differences between the FGT and VGT designs. It ensures the two turbocharger architectures have the same efficiency characteristics and swallowing capacity due to their identical base geometry. However, conducting an independent matching exercise with a catalogue of FGTs may find one with greater power recovery and in practice, a FGT is likely to exhibit higher efficiency due to its simpler design.

Secondly, the models used in this study only partially account for the effect of the high humidity of the exhaust flow from a fuel cell. The differences in the thermodynamic properties of the exhaust gas mixture are included, however, supersaturation of the water vapour leading to condensation forming in the turbine [37] is likely to occur in practical applications and is not accounted for. This will likely affect the absolute values of the results but is unlikely to affect the comparison of FGT and VGT, particularly considering that both turbines were found to operate at almost identical conditions after optimisation. Nevertheless, future work should consider the effects of condensation in the exhaust flow. The approach presented here could be combined with work by Zhang et al. [9] for example, who model turbine inlet flows with 100% humidity without condensation, and Mao et al. [38], who characterise the effects of nozzle gap on condensation formation, but not its subsequent

 doi:10.20944/preprints202503.0334.v1

implications on air system performance. Developing this research area may indicate other benefits for VGTs in managing fuel cell exhaust condensation and is of particular interest to the authors.

Finally, the study compares the steady state performance of both designs. Whilst steady state conditions represent much of fuel cell operation (which can be less transient than engines by using the onboard battery as a power buffer), future work should assess the performance of the two turbos under transient fuel cell conditions. Air path characteristics during transient loads could be particularly suitable to VGTs, which were found here to have greater flexibility under variable conditions.

Author Contributions: Conceptualization, D.D.B., R.B., and T.F.; methodology, A.F and M.L.S..; software, M.L.S., A.F, D.D.B. and T.F.; validation, D.D.B., and M.L.S.; formal analysis, M.L.S.; investigation, M.L.S.; writing—original draft preparation, A.F and M.L.S..; writing—review and editing, D.D.B., R.B., and T.F.; visualization, M.L.S. and T.F.; supervision, T.F.; project administration, T.F. and R.B.; funding acquisition, R.B. and T.F. All authors have read and agreed to the published version of the manuscript

Funding: This work was funded by the Advanced Propulsion Centre (APC) UK as part of the APC15 TRIDENT project. Matt Smith and Alex Fritot are supported by a scholarship from the EPSRC Centre for Doctoral Training in Advanced Automotive Propulsion Systems (AAPS), under the project EP/S023364/1.

Data Availability Statement: The original contributions presented in this study are included in the article/supplementary material. Further inquiries can be directed to the corresponding author(s).

Conflicts of Interest: The authors declare no conflicts of interest. The funders had no role in the design of the study; in the collection, analyses, or interpretation of data; in the writing of the manuscript; or in the decision to publish the results.

References

1. A. Elgowainy, *Electric, Hybrid, and Fuel Cell Vehicles*. New York: Springer, 2021. [Online]. Available: http://www.springer.com/series/15436
2. S. Atilhan, S. Park, M. M. El-Halwagi, M. Atilhan, M. Moore, and R. B. Nielsen, "Green hydrogen as an alternative fuel for the shipping industry," *Curr Opin Chem Eng*, vol. 31, Mar. 2021, doi: 10.1016/j.coche.2020.100668.
3. B. Heid, C. Martens, and M. Wilthaner, "Unlocking hydrogen's power for long-haul freight transport," *McKinsey*, Aug. 02, 2022.
4. B. Blunier and A. Miraoui, "Proton exchange membrane fuel cell air management in automotive applications," *J Fuel Cell Sci Technol*, vol. 7, no. 4, pp. 0410071–04100711, Aug. 2010, doi: 10.1115/1.4000627.
5. D. K. Kim *et al.*, "Efficiency improvement of a PEMFC system by applying a turbocharger," *Int J Hydrogen Energy*, vol. 39, no. 35, pp. 20139–20150, Dec. 2014, doi: 10.1016/j.ijhydene.2014.09.152.
6. W. Yu, S. Xu, and H. Ni, "Air Compressors for Fuel Cell Vehicles: An Systematic Review," *SAE International Journal of Alternative Powertrains*, vol. 4, no. 1, pp. 115–122, 2015, doi: https://doi.org/10.4271/2015-01-1172.
7. A. Kerviel, A. Pesyridis, A. Mohammed, and D. Chalet, "An evaluation of turbocharging and supercharging options for high-efficiency Fuel Cell Electric Vehicles," *Applied Sciences (Switzerland)*, vol. 8, no. 12, Dec. 2018, doi: 10.3390/app8122474.
8. A. Wiartalla, S. Pischinger, W. Bornscheuer, K. Fieweger, and J. Ogrzewalla, "Compressor Expander Units for Fuel Cell Systems," in *Fuel Cell Power for Transportation*, Detroit, Mar. 2000.
9. Y. Zhang, S. Xu, and C. Lin, "Performance improvement of fuel cell systems based on turbine design and supercharging system matching," *Appl Therm Eng*, vol. 180, Nov. 2020, doi: 10.1016/j.applthermaleng.2020.115806.
10. J. Hou, M. Yang, C. Ke, and J. Zhang, "Control logics and strategies for air supply in PEM fuel cell engines," *Appl Energy*, vol. 269, p. 115059, Jul. 2020, doi: 10.1016/J.APENERGY.2020.115059.
11. N. Ahmadi, A. Dadvand, S. Rezazadeh, and I. Mirzaee, "Analysis of the operating pressure and GDL geometrical configuration effect on PEM fuel cell performance," *Journal of the Brazilian Society of Mechanical Sciences and Engineering*, vol. 38, no. 8, pp. 2311–2325, Dec. 2016, doi: 10.1007/s40430-016-0548-0.

 doi:10.20944/preprints202503.0334.v1

12. Y. Qin, Q. Du, M. Fan, Y. Chang, and Y. Yin, "Study on the operating pressure effect on the performance of a proton exchange membrane fuel cell power system," *Energy Convers Manag*, vol. 142, pp. 357–365, 2017, doi: 10.1016/j.enconman.2017.03.035.
13. M. Amirinejad, S. Rowshanzamir, and M. H. Eikani, "Effects of operating parameters on performance of a proton exchange membrane fuel cell," *J Power Sources*, vol. 161, no. 2, pp. 872–875, Oct. 2006, doi: 10.1016/j.jpowsour.2006.04.144.
14. D. Hu, J. Liu, F. Yi, Q. Yang, and J. Zhou, "Enhancing heat dissipation to improve efficiency of two-stage electric air compressor for fuel cell vehicle," *Energy Convers Manag*, vol. 251, p. 115007, Jan. 2022, doi: 10.1016/J.ENCONMAN.2021.115007.
15. S. M. Milburn, J. J. Cronin, and B. M. Cohen, "A Variable Displacement Compressor/Expander for Vehicular Fuel Cell Air Management," in *Future Transportation Technology Conference*, Vancouver: SAE, Aug. 1995.
16. D. Zhao, L. Xu, Y. Huangfu, M. Dou, and J. Liu, "Semi-physical modeling and control of a centrifugal compressor for the air feeding of a PEM fuel cell," *Energy Convers Manag*, vol. 154, pp. 380–386, Dec. 2017, doi: 10.1016/j.enconman.2017.11.030.
17. M. Menze, M. Schoedel, and J. R. Seume, "Numerical Investigation of a Radial Turbine with Variable Nozzle Geometry for Fuel Cell Systems in Automotive Applications," in *14th European Conference on Turbomachinery Fluid Dynamics & Thermodynamics*, Gdansk, 2021. [Online]. Available: www.euroturbo.eu
18. S. Martinez-Boggio, D. Di Blasio, T. Fletcher, R. Burke, A. García, and J. Monsalve-Serrano, "Optimization of the air loop system in a hydrogen fuel cell for vehicle application," *Energy Convers Manag*, vol. 283, p. 116911, May 2023, doi: 10.1016/j.enconman.2023.116911.
19. N. Ahsan, A. Al Rashid, A. A. Zaidi, R. Imran, and S. Abdul Qadir, "Performance analysis of hydrogen fuel cell with two-stage turbo compressor for automotive applications," *Energy Reports*, vol. 7, pp. 2635–2646, Nov. 2021, doi: 10.1016/j.egyr.2021.05.007.
20. Y. Zhang, P. Bao, Y. Wan, and S. Xu, "Modeling and analysis of air supply system of polymer electrolyte membrane fuel cell system," *Energy Procedia*, vol. 142, pp. 1053–1058, Dec. 2017, doi: 10.1016/j.egypro.2017.12.355.
21. D. Filsinger, G. Kuwata, and N. Ikeya, "Tailored Centrifugal Turbomachinery for Electric Fuel Cell Turbocharger," *International Journal of Rotating Machinery*, vol. 2021, 2021, doi: 10.1155/2021/3972387.
22. C. Bao, M. Ouyang, and B. Yi, "Modeling and optimization of the air system in polymer exchange membrane fuel cell systems," *J Power Sources*, vol. 156, no. 2, pp. 232–243, Jun. 2006, doi: 10.1016/j.jpowsour.2005.06.008.
23. G. W. Kulp, S. Gurski, and D. J. Nelson, "PEM Fuel Cell Air Management Efficiency at Part Load," in *Future Car Congress*, 2002.
24. J. M. Cunningham, M. A. Hoffman, A. R. Eggert, and D. J. Friedman, "The Implications of Using an Expander (Turbine) in and Air System of a PEM Fuel Cell Engine," 2000.
25. R. Saidur, M. Rezaei, W. K. Muzammil, M. H. Hassan, S. Paria, and M. Hasanuzzaman, "Technologies to recover exhaust heat from internal combustion engines," Oct. 2012. doi: 10.1016/j.rser.2012.05.018.
26. A. J. Feneley, A. Pesiridis, and A. M. Andwari, "Variable Geometry Turbocharger Technologies for Exhaust Energy Recovery and Boosting-A Review," *Renewable and Sustainable Energy Reviews*, vol. 71, pp. 959–975, May 2017, doi: 10.1016/J.RSER.2016.12.125.
27. J. Liu, H. Wang, Z. Zheng, Z. Zou, and M. Yao, "Effects of Different Turbocharging Systems on Performance in a HD Diesel Engine with Different Emission Control Technical Routes," in *SAE Technical Papers*, SAE International, 2016. doi: 10.4271/2016-01-2185.
28. J. Cheong, S. Cho, and C. Kim, "Effect of Variable Geometry Turbocharger on HSDI Diesel Engine," in *Seoul 2000 FISITA World Automotive Congress*, Seoul, 2000.
29. M. Schoedel, M. Menze, and J. R. Seume, "Experimentally validated extension of the operating range of an electrically driven turbocharger for fuel cell applications," *Machines*, vol. 9, no. 12, Dec. 2021, doi: 10.3390/machines9120331.
30. A. H. Taylor, P. Naik, S. Nibler, and N. Al-Hasan, "Optimization of Variable Geometry Turbine Electric Turbocharger for a Heavy Duty, On-Highway Fuel Cell," in *ASME Turbo Expo*, 2023. [Online]. Available:

 doi:10.20944/preprints202503.0334.v1

http://asmedigitalcollection.asme.org/GT/proceedings-pdf/GT2023/87110/V13DT34A004/7046079/v13dt34a004-gt2023-101224.pdf?casa_token=FjiX3e16VWgAAAAA:KMKCtwnJLFUXUvmZcjJnEMDQR1cBmRSsWz1gPDPBIKR_y6fO82Bypeds6iHX6fGbuNDVhBA

31. P. Piqueras, J. de la Morena, E. J. Sanchis, and J. A. Lalangui, "Potential of Proton-Exchange Membrane Fuel-Cell System with On-Board O2-Enriched Air Generation," *Applied Sciences*, vol. 14, no. 2, p. 836, Jan. 2024, doi: 10.3390/app14020836.
32. Y. Zhao, Y. Liu, G. Liu, Q. Yang, L. Li, and Z. Gao, "Air and hydrogen supply systems and equipment for PEM fuel cells: a review," *Int J Green Energy*, vol. 19, no. 4, pp. 331–348, Mar. 2022, doi: 10.1080/15435075.2021.1946812.
33. C. Wang, Z. Xing, S. Sun, W. Chen, and Z. He, "Experimental study on the performance of oil-free twin-screw expanders for recovering energy in fuel cell systems," *Appl Therm Eng*, vol. 165, Jan. 2020, doi: 10.1016/j.applthermaleng.2019.114613.
34. N. C. Baines, *Fundamentals of Turbocharging*. White River Junction: Concepts NREC, 2005.
35. SAE International Recommended Practice, *J922 Turbocharger Nomenclature and Terminology*. 2011. doi: https://doi.org/10.4271/J922_201106.
36. SAE International Technical Standard, *J1826 Turbocharger Gas Stand Test Code*. 2022. doi: https://doi.org/10.4271/J1826_202204.
37. T. Wittmann, S. Lück, C. Bode, and J. Friedrichs, "On the Impact of Condensation and Liquid Water on the Radial Turbine of a Fuel Cell Turbocharger," *Machines*, vol. 10, no. 11, Nov. 2022, doi: 10.3390/machines10111053.
38. H. Mao, X. Tang, J. Liu, and S. Xu, "Numerical investigation of the non-equilibrium condensation inside a fuel cell turbine with variable geometry," *Int J Heat Mass Transf*, vol. 217, p. 124710, Dec. 2023, doi: 10.1016/j.ijheatmasstransfer.2023.124710.